Available online at www.sciencedirect.com
SCIENCE DIRECT®
Thin-Walled Structures 43 (2005) 273–290
THIN-WALLED STRUCTURES
www.elsevier.com/locate/tws

Dynamic buckling of a thin thermoviscoplastic rectangular plate

R.C. Batra*, Z. Wei

Department of Engineering Science and Mechanics, Virginia Polytechnic Institute and State University, MC 0219, Blacksburg, VA 24061, USA

Received 30 September 2003; accepted 26 July 2004
Available online 5 November 2004

Abstract

The dynamic buckling of a thin orthotropic thermoviscoplastic plate is studied by analyzing the stability of a stressed/deformed plate under superimposed infinitesimal perturbations. Elastic deformations are neglected. The wavelength of the perturbation that has the maximum initial growth rate is assumed to determine the buckled shape of the plate. The buckled shape of a rectangular plate loaded axially on two opposite edges thus ascertained is found to match well with the experimental findings.

Keywords: Perfectly plastic orthotropic plate; Buckling; Instability; Axial loading

1. Introduction

The buckling of thin rectangular plates under in-plane loads has been extensively studied, e.g. see Jones [1] for a review of the literature till 1989. The study of plastic buckling of plates began in late 1940s with the works of Illyshin [2], Stowell [3], and Bijlaard [4] who used the deformation theory of plasticity, and Handelman and Prager [5] who employed the incremental theory of plasticity. Pride and Heimerl [6] conducted buckling experiments on rectangular aluminum tubes and showed that predictions from the deformation theory of plasticity were closer to the test values than those from the incremental theory of plasticity. Pearson [7] showed that the assumption of no unloading

* Corresponding author. Tel.: +1 540 231 6051; fax: +1 540 231 4574.
E-mail addresses: rbatra@vt.edu (R.C. Batra), zwei@vt.edu (Z. Wei).

0263-8231/$ - see front matter © 2004 Elsevier Ltd. All rights reserved.
doi:10.1016/j.tws.2004.07.009

through the entire plate thickness improved predictions from the incremental theory of plasticity. Neale [8] showed that the buckling load was highly sensitive to imperfections. Needleman and Tvergaard [9], on the assumptions of a small initial imperfection and the axial stress at buckling being greater than the yield stress of the material, performed an asymptotic analysis to compute the buckling stress. Tvergaard [10] found that the buckling load is highly sensitive to the imposed strain rate, and the classic elastic–plastic buckling predictions are good approximations for small initial imperfections and low strain rates.

The effective stress at buckling in an isotropic rectangular plate loaded by in-plane tractions on two opposite edges only is greater than the yield stress of the material if the ratio of the thickness of the plate to the distance between the loaded edges exceeds $(3(1-\nu^2)\sigma_y/E)^{1/2}/\pi$ where σ_y, ν and E are the yield stress, Poisson's ratio and Young's modulus of the material, respectively [12]. For most engineering materials, this ratio equals about 0.03 which corresponds to thin plates.

Pauley and Aboudi [11], and Simiteses and Song [12] have used Bodner–Partom's theory of viscoplasticity without a yield surface to analyze elasto-plastic deformations of rectangular plates under in-plane compressive loads. Thus plastic deformations are assumed to always occur with the plastic strain rate depending upon the level of the effective stress. The computed buckling load depends upon the criterion used to define the buckled state of the plate.

Approximate analytical solutions can provide useful information and generally delineate the importance of various material and geometric parameters. Goodier [13], and Lindberg and Florence [14] have provided analytical and experimental values of mode shapes of a buckled plate. However, they did not explicitly state the buckling criterion employed. For a dynamically loaded elastic rectangular plate, Batra and Geng [15,16] assumed that the plate buckles when its transverse centroidal deflection equals three times the thickness. Here we postulate that if infinitesimal perturbations superimposed upon a deformed state grow in time, then the deformed state is unstable. The unstable deformed state corresponding to the maximum growth rate of the perturbation is taken to correspond to the buckled shape of the plate. The wavelength corresponding to the maximum growth rate of the perturbation gives the mode shape of the buckled plate. For different loading rates, the buckled mode shape is found to be close to that observed experimentally and also that given by Goodier [13]. Because of the neglect of elastic deformations, the buckling load cannot be determined.

2. Formulation of the problem

2.1. Governing equations

A schematic sketch of the problem studied and the location of the rectangular Cartesian coordinate axes used to describe infinitesimal deformations of a thin rectangular plate are shown in Fig. 1; the edges of the plate have lengths a and b, and its thickness equals h. It is assumed that deformations of the plate obey the Kirchhoff–Love hypotheses, and proportional loads N^0_{xx}, N^0_{yy} and N^0_{xy} are initially applied to the lateral edges of the plate so as to produce uniform stresses σ^0_{xx}, σ^0_{yy} and σ^0_{xy} and strain rates D^0_{xx}, D^0_{yy} and D^0_{xy}. The strain

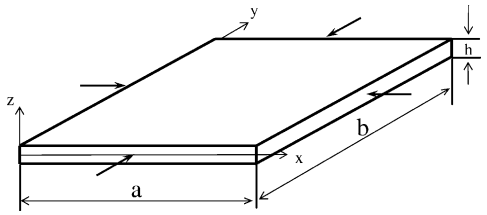

Fig. 1. Schematic sketch of thin plate.

rate in the plate during its subsequent deformations is given by

$$D_{xx} = D^0_{xx} + z\dot{k}_{xx},\ \dot{k}_{xx} = -\frac{\partial^2 \dot{w}}{\partial x^2},\ \dot{w} = \frac{\partial w}{\partial t},\quad D_{yy} = D^0_{yy} + z\dot{k}_{yy},$$

$$\dot{k}_{yy} = -\frac{\partial^2 \dot{w}}{\partial y^2},\quad D_{xy} = D^0_{xy} + z\dot{k}_{xy},\ \dot{k}_{xy} = -\frac{\partial^2 \dot{w}}{\partial x \partial y},\quad D^0_{xx} = \frac{\partial \dot{u}^0}{\partial x}, \tag{1}$$

$$D^0_{yy} = \frac{\partial \dot{v}^0}{\partial y},\ 2D^0_{xy} = \frac{\partial \dot{u}^0}{\partial y} + \frac{\partial \dot{v}^0}{\partial x},$$

where u, v and w are displacements of a point in the x, y and z directions, respectively. The transverse displacement, w, of the plate is given by

$$\frac{\partial^2 M_x}{\partial x^2} + 2\frac{\partial^2 M_{xy}}{\partial x \partial y} + \frac{\partial^2 M_y}{\partial y^2} + \left(N_x \frac{\partial^2 w}{\partial x^2} + 2N_{xy}\frac{\partial^2 w}{\partial x \partial y} + N_y \frac{\partial^2 w}{\partial y^2}\right) = \rho h \frac{\partial^2 w}{\partial t^2}, \tag{2}$$

where ρ is the mass density of the plate material, and

$$(M_x, M_y, M_{xy}) = \int_{-h/2}^{h/2} (\sigma_{xx}, \sigma_{yy}, \sigma_{xy}) z \, \mathrm{d}z, (N_x, N_y, N_{xy}) = \int_{-h/2}^{h/2} (\sigma_{xx}, \sigma_{yy}, \sigma_{xy}) \mathrm{d}z. \tag{3}$$

2.2. Constitutive relations

We assume that the plate is made of a homogeneous and orthotropic material with planes of material symmetry coincident with the coordinate planes, the material of the plate is rigid plastic, exhibits strain hardening, strain-rate hardening and thermal softening, the load at a material point is always increasing, and the transverse normal stress and the transverse shear stress are negligible. Thus Hill's [17] yield criterion may be written as

$$\phi \equiv \left[\frac{3}{2}\frac{(G+H)\sigma^2_{xx} - 2H\sigma_{xx}\sigma_{yy} + (F+H)\sigma^2_{yy} + 2N\sigma^2_{xy}}{F+G+H}\right]^{1/2} - \bar{\sigma} = 0, \tag{4}$$

where constants F, G, H and N characterize the orthotropic material, and $\bar{\sigma}$ is the equivalent yield stress of the material. For $N=3F=3G=3H$, Eq. (4) reduces to the von Mises yield criterion. For a material exhibiting strain hardening, strain-rate hardening and thermal softening, $\bar{\sigma}$ is a function of the effective plastic strain, the effective plastic strain

rate and the temperature. However, here we will assume that the effective plastic strain rate at a point is essentially constant and the heat conduction effects are negligible. Thus the incremental temperature rise, $\mathrm{d}\theta$, at a material point is given by

$$\mathrm{d}\theta = \beta\bar{\sigma}\,\mathrm{d}\bar{e}/(\rho c), \tag{5}$$

where c is the specific heat, β equals the fraction of the plastic working converted into heating, and $\mathrm{d}\bar{e}$ is the increment in the effective plastic strain $\bar{e}$. For $\dot{\bar{e}} = \text{const.}$, we assume that Eq. (5) can be solved for $\theta = \theta(\bar{e}, \bar{\sigma})$; one relation for which Eq. (5) can be integrated is given in Section 4. Hence the effective stress $\bar{\sigma}$ for locally adiabatic deformations at a constant strain rate can be expressed as a function of $\bar{e}$.

We assume that the material obeys the flow rule

$$D_{xx} = \lambda\frac{\partial\phi}{\partial\sigma_{xx}}, \quad D_{yy} = \lambda\frac{\partial\phi}{\partial\sigma_{yy}}, \quad D_{xy} = \lambda\frac{\partial\phi}{\partial\sigma_{xy}}, \tag{6}$$

where λ is a factor of proportionality. Substituting from (4) into (6), solving the resulting three equations for σ_{xx}, σ_{yy} and σ_{xy}, defining the equivalent plastic strain rate, $\dot{\bar{e}}$, by

$$\sigma_{xx}D_{xx} + \sigma_{yy}D_{yy} + 2\sigma_{xy}D_{xy} = \bar{\sigma}\dot{\bar{e}}, \tag{7}$$

we obtain

$$\begin{aligned}
\sigma_{xx} &= \frac{2}{3}\bar{\sigma}/\dot{\bar{e}}\frac{(F+G+H)}{(FG+GH+HF)}[(F+H)D_{xx} + HD_{yy}], \quad \sigma_{yy} \\
&= \frac{2}{3}\bar{\sigma}/\dot{\bar{e}}\frac{(F+G+H)}{(FG+GH+HF)}[(G+H)D_{yy} + HD_{xx}], \quad \sigma_{xy} \\
&= \frac{2}{3}\bar{\sigma}/\dot{\bar{e}}\frac{(F+G+H)}{N}D_{xy}.
\end{aligned} \tag{8}$$

It can be shown that

$$\dot{\bar{e}} = \lambda = \left[\frac{2}{3}(AD_{xx}^2 + BD_{yy}^2 + CD_{xx}D_{yy} + DD_{xy}^2)\right]^{1/2}, \tag{9}$$

where

$$\begin{aligned}
A &= \frac{(F+G+H)(F+H)}{(FG+GH+HF)}, \quad B = \frac{(F+G+H)(G+H)}{(FG+GH+HF)}, \\
C &= \frac{2(F+G+H)H}{(FG+GH+HF)}, \quad D = \frac{2(F+G+H)}{N}.
\end{aligned} \tag{10}$$

2.3. Simplification of the governing equations

Substituting from (1) into (9) and neglecting terms multiplying z^2, we obtain

$$\dot{\bar{e}}^2 = \dot{\bar{e}}_0^2 + \frac{4}{3}\left[AD_{xx}^0\dot{k}_{xx} + BD_{yy}^0\dot{k}_{yy} + \frac{C}{2}(D_{xx}^0\dot{k}_{yy} + D_{yy}^0\dot{k}_{xx}) + D_{xy}^0\dot{k}_{xy}\right]z, \tag{11}$$

where $\dot{\bar{e}}_0$ is obtained from $\dot{\bar{e}}$ by setting $D_{xx} = D^0_{xx}$, etc. Since $|\dot{k}_{xx}|$, $|\dot{k}_{yy}|$ and $|\dot{k}_{xy}|$ multiplied by $h/\dot{\bar{e}}_0$ are all much smaller than 1, therefore,

$$\dot{\bar{e}} = \dot{\bar{e}}_0 + \frac{2}{3}\left[AD^0_{xx}\dot{k}_{xx} + BD^0_{yy}\dot{k}_{yy} + \frac{C}{2}(D^0_{xx}\dot{k}_{yy} + D^0_{yy}\dot{k}_{xx}) + D^0_{xy}\dot{k}_{xy}\right] z/\dot{\bar{e}}_0. \tag{12}$$

Integration of Eq. (12) with respect to time gives

$$\bar{e} = \bar{e}_0 + \frac{2}{3}\left[AD^0_{xx}k_{xx} + BD^0_{yy}k_{yy} + \frac{C}{2}(D^0_{xx}k_{yy} + D^0_{yy}k_{xx}) + D^0_{xy}k_{xy}\right] z/\dot{\bar{e}}_0. \tag{13}$$

Recalling that the initial state of deformation obeys the flow rule (6), we use Eqs. (4), (6) and (8) to substitute in Eq. (13) for D^0_{xx}, D^0_{yy} and D^0_{xy} in terms of σ^0_{xx}, σ^0_{yy} and σ^0_{xy} and arrive at the following:

$$\bar{e} = \bar{e}_0 + \frac{z}{\bar{\sigma}^0}(\sigma^0_{xx}k_{xx} + \sigma^0_{yy}k_{yy} + 2\sigma^0_{xy}k_{xy}), \tag{14}$$

where $\bar{\sigma}^0$ is the initial equivalent stress given by Eq. (4) with σ_{xx}, σ_{yy}, etc. replaced by initial stresses σ^0_{xx}, σ^0_{yy}. For small deformations, the relation $\bar{\sigma} = \bar{\sigma}(\bar{e})$ can be approximated by

$$\bar{\sigma} = \bar{\sigma}|_{\bar{e}=0} + \frac{\mathrm{d}\bar{\sigma}}{\mathrm{d}\bar{e}}|_{\bar{e}=0}\bar{e} = \bar{\sigma}|_{\bar{e}=0} + E(\bar{e})\bar{e}, \tag{15}$$

where $E(\bar{e})$ is the tangent modulus; e.g. see Fig. 2. Eq. (15) is exact for a rigid plastic linearly strain hardening material deformed at a constant strain rate and at a uniform temperature.

Substitution from (14) into (15) gives

$$\bar{\sigma} = \bar{\sigma}^0 + \frac{E(\bar{e})z}{\bar{\sigma}^0}[\sigma^0_{xx}k_{xx} + \sigma^0_{yy}k_{yy} + 2\sigma^0_{xy}k_{xy}]. \tag{16}$$

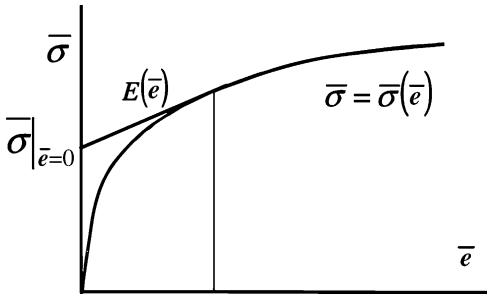

Fig. 2. Schematic diagram of the stress–strain curve.

We now substitute into Eq. (8) for strain rates from Eq. (1), for $\dot{\bar{e}}$ from Eq. (12) and for $\bar{\sigma}$ from Eq. (16) to arrive at the following equations:

$$\begin{aligned}
\sigma_{xx} &= \sigma_{xx}^0 + z\Big\{E\alpha(\alpha k_{xx} + \beta k_{yy} + 2\gamma k_{xy}) + \frac{1}{\lambda_0}\Big[\Big(A - \frac{3}{2}\alpha^2\Big)\dot{k}_{xx} \\
&\quad + \Big(\frac{C}{2} - \frac{3}{2}\alpha\beta\Big)\dot{k}_{yy} - 3\gamma\alpha\dot{k}_{xy}\Big]\Big\}, \\
\sigma_{yy} &= \sigma_{yy}^0 + z\big\{E\beta(\alpha k_{xx} + \beta k_{yy} + 2\gamma k_{xy}) \\
&\quad + \frac{1}{\lambda_0}\Big[\Big(\frac{C}{2} - \frac{3}{2}\beta\alpha\Big)\dot{k}_{xx} + \Big(B - \frac{3}{2}\beta^2\Big)\dot{k}_{yy} - 3\gamma\beta\dot{k}_{xy}\Big]\Big\}, \\
\sigma_{xy} &= \sigma_{xy}^0 + z\Big\{E\gamma(\alpha k_{xx} + \beta k_{yy} + 2\gamma k_{xy}) + \frac{1}{\lambda_0}\Big[-\frac{3}{2}\gamma(\alpha\dot{k}_{xx} + \beta\dot{k}_{yy}) \\
&\quad + \Big(\frac{D}{2} - 3\gamma^2\Big)\dot{k}_{xy}\Big]\Big\},
\end{aligned} \tag{17}$$

where

$$\alpha = \frac{\sigma_{xx}^0}{\bar{\sigma}^0},\ \ \beta = \frac{\sigma_{yy}^0}{\bar{\sigma}^0},\ \ \gamma = \frac{\sigma_{xy}^0}{\bar{\sigma}^0},\ \ \lambda_0 = 3\dot{\bar{e}}_0. \tag{18}$$

Substitution from (17) into (3) and the result into (2) yield the following equation for the transverse deflection w:

$$\begin{aligned}
&(2A - 3\alpha^2)\frac{\partial^4\dot{w}}{\partial x^4} - 12\alpha\gamma\frac{\partial^4\dot{w}}{\partial x^3\partial y} + [2C - 6\alpha\beta + 2(D - 6\gamma^2)]\frac{\partial^4\dot{w}}{\partial x^2\partial y^2} \\
&\quad - 3\beta\gamma[D + 2]\frac{\partial^4\dot{w}}{\partial x\partial y^3} + [2B - 3\beta^2]\frac{\partial^4\dot{w}}{\partial y^4} + 2E(\bar{e})\lambda_0\Big\{\alpha^2\frac{\partial^4 w}{\partial x^4} + 4\alpha\gamma\frac{\partial^4 w}{\partial x^3\partial y} \\
&\quad + 2(\alpha\beta + 2\gamma^2)\frac{\partial^4 w}{\partial x^2\partial y^2} + 4\beta\gamma\frac{\partial^4 w}{\partial x\partial y^3} + \beta^2\frac{\partial^4 w}{\partial y^4}\Big\} - \Big(\sigma_{xx}^0\frac{\partial^2 w}{\partial x^2} + 2\sigma_{xy}^0\frac{\partial^2 w}{\partial x\partial y} \\
&\quad + \sigma_{yy}^0\frac{\partial^2 w}{\partial y^2}\Big)\frac{24\lambda_0}{h^2} + \frac{24\lambda_0}{h^2}\rho\ddot{w} = 0.
\end{aligned} \tag{19}$$

When the initial shear stress σ_{xy}^0 vanishes, then $\gamma = 0$ from third of Eq. (18) and Eq. (19) is reduced to

$$\begin{aligned}
&\Big(Q_1\frac{\partial^4\dot{w}}{\partial x^4} + Q_2\frac{\partial^4\dot{w}}{\partial x^2\partial y^2} + Q_3\frac{\partial^4\dot{w}}{\partial y^4}\Big) + 2E(\bar{e})\lambda_0\Big(\alpha^2\frac{\partial^4 w}{\partial x^4} + 2\alpha\beta\frac{\partial^4 w}{\partial x^2\partial y^2} + \beta^2\frac{\partial^4 w}{\partial y^4}\Big) \\
&\quad - \frac{24\lambda_0}{h^2}\Big(\sigma_{xx}^0\frac{\partial^2 w}{\partial x^2} + \sigma_{yy}^0\frac{\partial^2 w}{\partial y^2}\Big) + \frac{24\lambda_0}{h^2}\rho\ddot{w} = 0,
\end{aligned} \tag{20}$$

where

$$Q_1 = 2A - 3\alpha^2, \quad Q_2 = 2(C - 3\alpha\beta + D), \quad Q_3 = 2B - 3\beta^2. \tag{21}$$

The first group of terms involving $\dot{w}$ represents the directional moment resistance, the second group of terms multiplying $E(\bar{e})$ and containing fourth order partial derivatives of w with respect to the spatial coordinates represents the effect of strain hardening, the third

group of terms containing σ^0_{xx} and σ^0_{yy} represents the axial thrust causing buckling, and the fourth term accounts for the resistance to buckling offered by inertia forces. Henceforth we assume that the initial shear stress σ^0_{xy} vanishes.

3. Buckling deformations

In order to find the buckling load we perturb the deformed state of the plate by an infinitesimal amount. If the superimposed perturbations grow in time, then the ground state is unstable. The buckled shape of the plate corresponds to the wavelength of the perturbation that results in the maximum initial growth rate of the perturbation.

Let $w_0(x, y) = w(x, y, t_0)$ give the deflection of the plate at time $t = t_0$, and it be given an infinitesimal perturbation $\delta w(x, y, t)$ where $\sup|\delta w/w_0| \ll 1$ and $\sup|\delta \dot{w}/\dot{w}_0| \ll 1$. We assume that the resultant forces and moments of forces are unaffected by the superimposed perturbation. Also, the perturbation field satisfies the following boundary conditions at the edges of the simply supported plate:

$$\delta w(0, y, t) = \delta w(a, y, t) = 0, \quad \delta w(x, 0, t) = \delta w(x, b, t) = 0; \quad \frac{\partial^2 \delta w}{\partial x^2}\Big|_{(0,y,t)} = 0,$$
$$\frac{\partial^2 \delta w}{\partial x^2}\Big|_{(a,y,t)} = 0, \quad \frac{\partial^2 \delta w}{\partial y^2}\Big|_{(x,0,t)} = 0, \quad \frac{\partial^2 \delta w}{\partial y^2}\Big|_{(x,b,t)} = 0. \tag{22}$$

The perturbation field

$$\delta w(x, y, t) = \delta w^* e^{\eta(t-t_0)} \sin \omega_1 x \sin \omega_2 y, \quad \omega_1 = \frac{2\pi n}{a}, \quad \omega_2 = \frac{2\pi m}{b}, \tag{23}$$

where m and n are integers, satisfies boundary conditions (22). Note that any spatial variation of a perturbation field can be expressed as the sum of a double Fourier series; thus it suffices to consider perturbations of the form (23). In Eq. (23), η is the initial growth rate of the perturbation at time $t = t_0$. A positive value of η implies that the deformed plate at time t_0 is unstable; otherwise it is stable. Substituting $w = w_0 + \delta w$ into Eq. (20) and subtracting (20) from the resulting equation, we get the following algebraic equation relating wavenumbers ω_1 and ω_2 to the growth rate η.

$$\frac{24\lambda_0}{h^2}\rho\eta^2 + (Q_1\omega_1^4 + Q_2\omega_1^2\omega_2^2 + Q_3\omega_2^4)\eta + 2E(\bar{e})\lambda_0(\alpha^2\omega_1^4 + 2\alpha\beta\omega_1^2\omega_2^2 + \beta^2\omega_2^4)$$
$$+ \frac{24\lambda_0}{h^2}(\sigma^0_{xx}\omega_1^2 + \sigma^0_{yy}\omega_2^2) = 0. \tag{24}$$

We now consider extreme values of the wavenumbers. We note that

$$\omega_1 = \omega_2 = 0 \Rightarrow \eta = 0, \quad \omega_1 = \omega_2 = \infty \Rightarrow \eta = -\frac{2E(\bar{e})\lambda_0(\alpha^2 + 2\alpha\beta + \beta^2)}{Q_1 + Q_2 + Q_3} < 0,$$
$$\omega_1 = 0,\ \omega_2 = \infty \Rightarrow \eta = -\frac{2E(\bar{e})\lambda_0\beta^2}{Q_3} < 0, \quad \omega_1 = \infty,$$
$$\omega_2 = 0 \Rightarrow \eta = -\frac{2E(\bar{e})\lambda_0\alpha^2}{Q_1} < 0. \tag{25}$$

Thus for extreme values of wavenumbers of the perturbation, the deformed configuration of the plate is stable. However, for some finite nonzero values of ω_1 and ω_2, the growth rate η of the perturbation may be positive. Values of ω_1 and ω_2 that result in the extremum values of η are solutions of the following two equations.

$$\begin{aligned}
&\frac{\partial\eta}{\partial\omega_1} = 0 \Rightarrow \eta(2Q_1\omega_1^2 + Q_2\omega_2^2) + 2E(\bar{e})\lambda_0(2\omega_1^2\alpha^2 + 2\alpha\beta\omega_2^2) + \frac{24\lambda_0}{h^2}\sigma_{xx}^0 = 0,\\
&\frac{\partial\eta}{\partial\omega_2} = 0 \Rightarrow \eta(Q_2\omega_1^2 + 2Q_3\omega_2^2) + 2E(\bar{e})\lambda_0(2\alpha\beta\omega_1^2 + 2\beta^2\omega_2^2) + \frac{24\lambda_0}{h^2}\sigma_{yy}^0 = 0.
\end{aligned} \tag{26}$$

Eqs. (24) and (26) comprise three equations for the determination of ω_1, ω_2 and η. An analytical solution of these equations, if it can be obtained with Mathematica, may not shed much light on the relative importance of various variables in determining the buckled shape of the plate. Accordingly, we consider the simpler case of a plate loaded only on two opposite edges.

3.1. Uniaxial impact load

Let the plate be compressed in the x-direction by applying uniformly distributed loads on the edges $x=0$ and $x=a$, and the initial stress be given by

$$\sigma_{xx}^0 = -\left(\frac{2}{3}\frac{F+G+H}{G+H}\right)^{1/2}\sigma_0, \quad \sigma_0 > 0, \quad \sigma_{yy}^0 = \sigma_{xy}^0 = 0. \tag{27}$$

Therefore, from Eqs. (4) and (18),

$$\alpha = -\left(\frac{2}{3}\frac{F+G+H}{G+H}\right)^{1/2}, \quad \beta = 0, \quad \gamma = 0. \tag{28}$$

The initial strain rates are given by

$$D_{xx}^0 = \frac{1}{\alpha}\dot{\bar{e}}_0, \quad D_{yy}^0 = \left(\frac{3H^2}{2(F+G+H)(G+H)}\right)^{1/2}\dot{\bar{e}}_0, \quad D_{xy}^0 = 0, \quad \dot{\bar{e}}_0 > 0. \tag{29}$$

The problem can be further simplified if we assume that buckling deformations are independent of the y-coordinate. Experimental work of Goodier [13] supports this assumption. Eq. (24) then simplifies to

$$\frac{24\lambda_0}{h^2}\rho\eta^2 + Q_1\omega_1^4\eta + 2E(\bar{e})\lambda_0\alpha^2\omega_1^4 + \frac{24\lambda_0\alpha}{h^2}\sigma_0\omega_1^2 = 0. \tag{30}$$

The equation $\partial\eta/\partial\omega_1 = 0$ gives

$$\omega_1^2 = -\frac{\alpha\sigma_0^2}{2(Q_1\eta + 2E(\bar{e})\lambda_0\alpha^2)}\frac{24\lambda_0}{h^2} \quad \text{or} \quad \eta = -\frac{\frac{24\lambda_0\alpha}{h^2}\sigma_0 + 4E(\bar{e})\alpha^2\lambda_0\omega_1^2}{2Q_1\omega_1^2}. \tag{31}$$

Substitution for ω_1^2 from (31) into (30) gives

$$\rho\eta^2 = \frac{\alpha^2\sigma_0^2}{4(Q_1\eta + 2E(\bar{e})\lambda_0\alpha^2)}\frac{h^2\lambda_0}{24}. \tag{32}$$

We set $F_1 = \rho\eta^2$, and

$$F_2 = \frac{\alpha^2\sigma_0^2}{4(Q_1\eta + 2E(\bar{e})\lambda_0\alpha^2)}\frac{h^2\lambda_0}{24}.$$

The fourth of Eq. (18) implies that $\lambda_0 > 0$. For $Q_1 > 0$, F_1 and F_2 are schematically plotted against η in Fig. 3. The point of intersection of the two curves gives a solution of Eq. (32). For $Q_1 > 0$, $\eta > 0$ is a solution of Eq. (32), and the initial deformed state becomes unstable as soon as the material starts deforming plastically. This is because elastic deformations have been neglected. We now attempt to find the buckled shape.

In terms of nondimensional variables

$$\bar{\eta} = \eta/\dot{\bar{e}}_0, \quad \bar{\omega} = L\omega_1, \tag{33}$$

where L is a characteristic length, Eqs. (30) and (31) yield

$$\bar{\eta}^3 + a_1\bar{\eta}^2 - c_1 = 0, \quad \text{or} \quad \bar{\omega}^3 + a_2\bar{\omega}^2 - c_2 = 0, \tag{34}$$

where

$$a_1 = \frac{(R+1)E(\bar{e})}{R^2\bar{\sigma}_0}, \qquad c_1 = \frac{3\bar{\sigma}_0(2R+1)}{\rho R^2\dot{\bar{e}}_0^2 h^2}, \tag{35}$$

$$a_2 = \frac{\sqrt{2}(2R+1)LE(\bar{e})\dot{\bar{e}}_0}{\sqrt{-\alpha}R^2\bar{\sigma}_0\sqrt{\bar{\sigma}_0/\rho}}, \quad c_2 = \frac{9\sqrt{2}(2R+1)\sqrt{-\alpha}(R+1)}{R^2(R+2)h^2}\frac{L^3\dot{\bar{e}}}{\sqrt{\bar{\sigma}_0/\rho}}, \tag{36}$$

$$R = \frac{H}{F} = \frac{H}{G}.$$

A real solution of the first of cubic Eq. (34) is

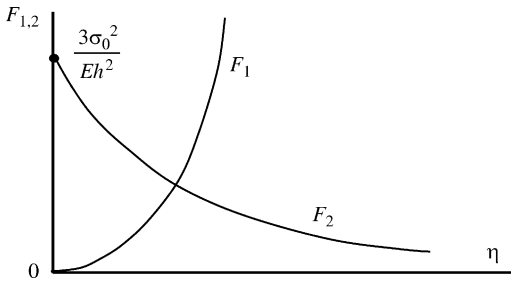

Fig. 3. Schematic plots of functions F_1 and F_2 defined immediately after Eq. (32).

$$\bar{\eta}=\dot{\bar{e}}_0\left[\left(-\frac{q_1}{2}+\left(\left(\frac{p_1}{3}\right)^3+\left(\frac{q_1}{2}\right)^2\right)^{1/2}\right)^{1/3}+\left(-\frac{q_1}{2}-\left(\left(\frac{p_1}{3}\right)^3+\left(\frac{q_1}{2}\right)^2\right)^{1/2}-\frac{a_1}{3}\right)\right], \tag{37}$$

where

$$p_1=-a_1^2/3,\quad q_1=2(a_1/3)^3-c_1. \tag{38}$$

A real solution of the second of cubic Eq. (34) for the dimensional wavenumber $\bar{\omega}=\bar{\omega}_1$ is

$$\bar{\omega}=\left[\left(-\frac{q_2}{2}+\left(\left(\frac{p_2}{3}\right)^3+\left(\frac{q_2}{2}\right)^2\right)^{1/2}\right)^{1/3}+\left(-\frac{q_2}{2}-\left(\left(\frac{p_2}{3}\right)^3+\left(\frac{q_2}{2}\right)^2\right)^{1/2}-\frac{a_2}{3}\right)\right]/L, \tag{39}$$

where

$$p_2=-a_2^2/3,\quad q_2=2\left(\frac{a_2}{3}\right)^3-c_2. \tag{40}$$

For most materials, the order of magnitude of different material parameters is

$$\begin{aligned}&\rho\sim 10^3\ \text{kg/m}^3,\quad R\sim 1,\quad \bar{\sigma}_0\sim 10^2\ \text{to}\ 10^3\ \text{MPa},\\ &\dot{\bar{e}}_0\sim 10\ \text{to}\ 10^3/\text{s},\quad E(\bar{e})/\bar{\sigma}_0\sim 1,\quad h\sim 1\ \text{mm},\quad a_1\sim 10^{-1},\quad a_2\sim 10^{-3}.\end{aligned} \tag{41}$$

For $a_1\ll 1$ and $a_2\ll 1$, one can expand solutions of the first of Eq. (34) and the second part of Eq. (34) as power series in a_1 and a_2. That is,

$$\bar{\eta}=\bar{\eta}_0+a_1\bar{\eta}_1+O(a_1^2),\quad \bar{\omega}=\bar{\omega}_0+a_2\bar{\omega}_1+O(a_2^2). \tag{42}$$

Substitution from (42) into (34), equating all terms with different orders of small parameters, and converting the solution to dimensional variables, we get

$$\begin{aligned}\eta&=\left[\left(\frac{3\bar{\sigma}_0(2R+1)\dot{\bar{e}}_0}{\rho R^2h^2}\right)^{1/3}-\frac{(2R+1)E(\bar{e})\dot{\bar{e}}_0}{3R^2\bar{\sigma}_0}\right],\\ \omega&=\left(\frac{9\sqrt{-2\alpha}(2R+1)(R+1)\dot{\bar{e}}_0}{R^2(R+2)\sqrt{\bar{\sigma}_0/\rho}h^2}\right)^{1/3}-\frac{\sqrt{2}(2R+1)E(\bar{e})\dot{\bar{e}}_0}{\sqrt{-\alpha}(3R^2\bar{\sigma}_0)\sqrt{\bar{\sigma}_0/\rho}}.\end{aligned} \tag{43}$$

For an isotropic material, $R=1$, $\alpha=-1$, and Eq. (43) simplifies to

$$\eta=\left[\left(\frac{9\bar{\sigma}_0\dot{\bar{e}}_0}{\rho h^2}\right)^{1/3}-\frac{E(\bar{e})\dot{\bar{e}}_0}{\bar{\sigma}_0}\right],\quad \omega=\left(\frac{18\sqrt{2}\dot{\bar{e}}_0}{\sqrt{\bar{\sigma}_0/\rho}h^2}\right)^{1/3}-\frac{\sqrt{2}E(\bar{e})\dot{\bar{e}}_0}{\bar{\sigma}_0\sqrt{\bar{\sigma}_0/\rho}}. \tag{44}$$

For an isotropic perfectly plastic material,

$$\eta = \left(\frac{9\bar{\sigma}_0\dot{\bar{e}}_0}{\rho h^2}\right)^{1/3}, \quad \omega = \left(\frac{18\sqrt{2}\dot{\bar{e}}_0}{\sqrt{\bar{\sigma}_0/\rho}h^2}\right)^{1/3}. \tag{45}$$

Eq. (43) implies that the strain hardening of the material decreases the maximum growth rate and the associated wavenumber of perturbations. The magnitude of the first term in the first of Eq. (43) is very large as compared to that of the second term. Had we kept second-order terms in (42), then η would have always come out to be positive as for the solution of Eq. (32). The second of Eq. (43) exhibits the dependence of the buckled shape of the plate upon the applied effective strain rate, the effective stress at yield, the mass density, the plate thickness and the strain hardening modulus. The wavenumber of the buckled shape varies as $h^{-2/3}$ signifying that a thin plate will have less wigly buckled shape than a thick plate.

The integer closest to $a\omega/\pi$ determines the buckled shape of the plate.

4. Results and discussion

For an isotropic strain-hardening material, we have compared in Table 1 the buckled mode shape computed from the second of Eq. (43) with the experimental values and also with those computed by Goodier [13] using a modal method. It is clear that buckled shapes computed from the present analysis are close to those observed experimentally, and also to those given by Goodier [13]. For a perfectly plastic isotropic or orthotropic material, η and ω vary as $(\dot{\bar{e}}_0)^{1/3}$. Thus $\eta \to 0$ and $\omega \to 0$ as $\dot{\bar{e}}_0 \to 0$. That is, even a perturbation of very small wavenumber will destabilize a simply supported isotropic perfectly plastic plate deformed quasistatically. This is because elastic deformations have been neglected. Eqs. (43) and (45) reveal that the wavenumber of the destabilizing perturbation decreases with an increase in $\bar{\sigma}_0$ and h, and its growth rate increases with an increase in $\bar{\sigma}_0$ and a decrease in h. For a strain hardening material, the first of Eqs. (43) and (44) at first glance suggest that η may not be positive. However, the magnitude of the first term is much larger than that of the second term, and η is always positive.

Results presented in Figs. 4–6 are for the SAC-1 plate of Table 1. For different values of the applied axial strain rate, Fig. 4 compares the maximum growth rate of the perturbation and the corresponding wavenumber as computed from the exact solutions (37) and (39) and the asymptotic solution (43). The growth rates computed from the exact and the asymptotic solutions agree with each other. The exact and the asymptotic solutions for the wavenumber agree qualitatively, and the difference between the two increases with an increase in the applied axial strain rate. For a strain rate of 2000/s, the difference between the two wavenumbers equals 2%. For each solution, the maximum growth rate and the corresponding wavenumber increase with an increase in the strain rate. Results plotted in Fig. 5 reveal that the maximum growth rate of the perturbation decreases by 16% for an 8-fold increase in the value of the hardening modulus; the corresponding wavenumber decreases by only 5%.

Table 1
Comparison of computed and observed number of half waves during buckling of a simply supported rectangular plate; experimental data from [13]

Specimen	Width b (cm)	Thickness (cm)	Yield stress (MPa)	Hardening modulus (GPa)	Axial velocity (m/s)	Strain rate (1/s)	Shortening (%)	Mode (exp. [13])	Mode (Goodier) [13]	Mode (present model)
SAC-1	1.27	0.159	207	333	122	961	36	16	14	13
SAC-2	1.27	0.159	207	333	91	717	23	19	14	12
SAC-3	1.27	0.159	207	333	61	480	10	19	14	10
SAC-4	1.27	0.318	207	333	176	1386	29	13	14	9
LAC-1	1.91	0.159	198	404	56	441	7	13	9	10
LAC-2	1.91	0.159	207	333	94	756	16	12	9	12
LAC-3	1.91	0.159	207	333	105	827	30	14	9	12
LAC-4	1.91	0.318	207	333	115	906	15	14	9	8
LAC-5	1.91	0.318	207	333	140	1102	20	10	9	8
4CSC-1	1.91	0.159	177	839	35	276	3	10	8	9
4CSC-2	1.91	0.159	177	839	30	236	3	10	7	8
4CSC-3	1.91	0.159	177	1792	18	142	1	8	6	7

All plates of length $a = 12.7$ cm.

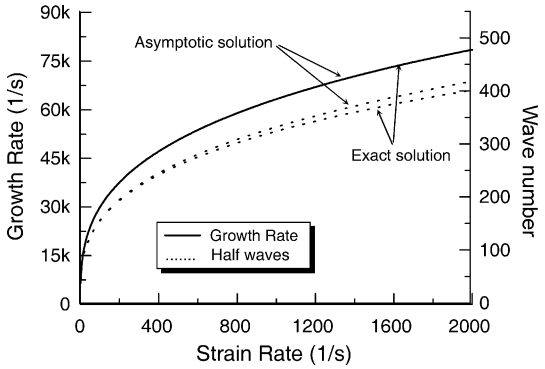

Fig. 4. The dependence upon the axial strain rate of the maximum initial growth rate and the corresponding number of half-wavelengths along the plate length as found from the exact and the asymptotic solutions.

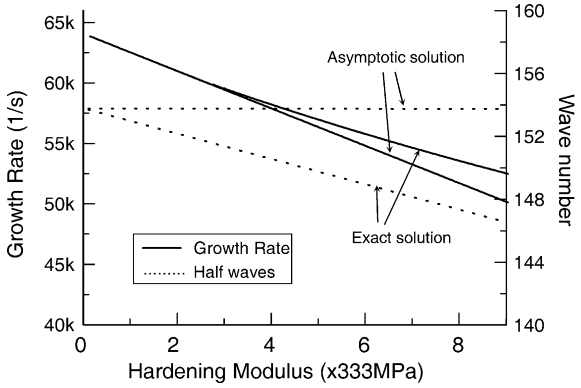

Fig. 5. The dependence upon the hardening modulus of the maximum initial growth rate and the corresponding number of half-wavelengths along the plate length as found from the exact and the asymptotic solutions.

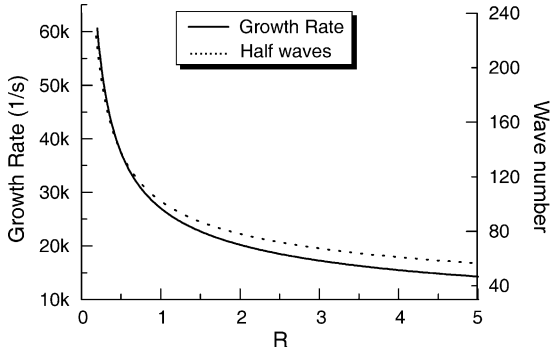

Fig. 6. The dependence of the maximum initial growth rate and the corresponding number of half-wavelengths along the plate length upon the factor, R, of normal anisotropy.

Fig. 6 exhibits the effect of the normal anisotropy parameter, R, upon the maximum growth rate and the corresponding wavenumber of the perturbations. The wavenumber of the buckled plate decreases monotonically and exponentially with an increase in the value of R. Thus the buckled shape of a highly anisotropic plate will differ significantly from that of an isotropic plate.

In order to compute results for an isotropic thermoviscoplastic plate we assume that the material obeys the following relation among the effective stress $\bar{\sigma}$, the effective plastic strain $\bar{e}$, the effective plastic strain rate $\dot{\bar{e}}$, and the temperature θ; e.g. see [18] where it is referred to as the Litonski–Batra thermoviscoplastic relation.

$$\bar{\sigma} = \hat{\sigma}_0 \left(1 + \frac{\bar{e}}{e_y}\right)^n (1 + b\dot{\bar{e}})^m \left(\frac{\theta - \theta_r}{\theta_m - \theta_r}\right). \tag{45}$$

Substitution from (46) into (5) and integrating the resulting equation, we get

$$\theta - \theta_m = (\theta_m - \theta_r)\exp\left\{\frac{\beta\hat{\sigma}_0 e_y (1 + b\dot{\bar{e}})^m}{\rho c(\theta_m - \theta_r)(1+n)}\left[\left(1 + \frac{\bar{e}}{e_y}\right)^{n+1} - 1\right]\right\}. \tag{46}$$

Values assigned to material parameters $\hat{\sigma}_0$, e_y, b, n, m and θ_m are listed in Table 2; in Eq. (46) θ_r is the room temperature.

We now delineate the effect of material parameters in the thermoviscoplastic relation (46) on the maximum growth rate of perturbations and the corresponding wavenumber. We set $\beta = 1$ thereby assuming that all the plastic working is converted into heating. The material of the plate is isotropic, and values of material and geometric parameters, except for the parameter being varied, are listed in Table 2. The strain hardening modulus $E(\bar{e}) = \mathrm{d}\bar{\sigma}/\mathrm{d}\bar{e}$ can be computed from Eqs. (46) and (47) by using

$$E(\bar{e}) = \frac{\partial\bar{\sigma}}{\partial\bar{e}} + \frac{\partial\bar{\sigma}}{\partial\theta}\frac{\mathrm{d}\theta}{\mathrm{d}\bar{e}}.$$

Figs. 7–10 exhibit the influence upon the maximum initial growth rate and the corresponding wavenumber of the applied strain rate, the plate thickness, strain rate hardening exponent and the strain hardening exponent. Results have been computed by using the analytical solutions (37) and (39). The wavenumber increases monotonically with an increase in the applied strain rate but decreases with an increase in the plate thickness, strain-rate hardening exponent and the strain hardening exponent. Thus the wavelength of the buckled plate will increase with an increase in the plate

Table 2
Values of material parameters

Material	$\hat{\sigma}_0$ (MPa)	n	m	ρ (kg/m^3)	c (J/kg K)	e_y	β	$\dot{\bar{e}}_0$ (1/s)	θ_m (K)	θ_r (K)	b (1/s)	h (m)
HY-100 Steel	207	0.107	0.0117	7860	473	0.007	0.9	100	1500	300	17320	0.0025

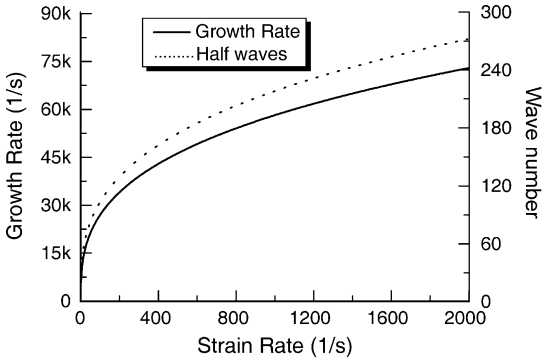

Fig. 7. The dependence of the maximum initial growth rate and the corresponding number of half-wavelengths along the plate length upon the initial axial strain rate.

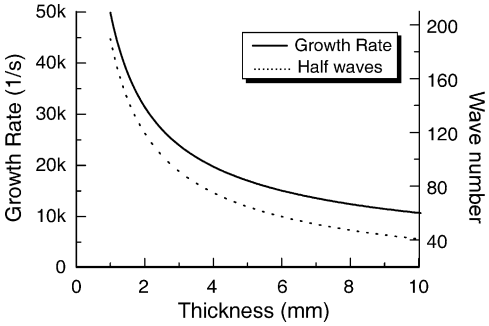

Fig. 8. The dependence of the maximum initial growth rate and the corresponding number of half-wavelengths along the plate length upon the plate thickness.

thickness. For a 10-fold increase in the strain-rate from 200/s to 2000/s, the wavenumber increases by a factor of 2. A 10-fold increase in the plate thickness from 1 to 10 mm, the wavenumber of the buckled plate decreases by a factor of 4.5. However, a 10-fold increase in the strain-rate hardening exponent from 0.0117 to 0.117, and in strain hardening

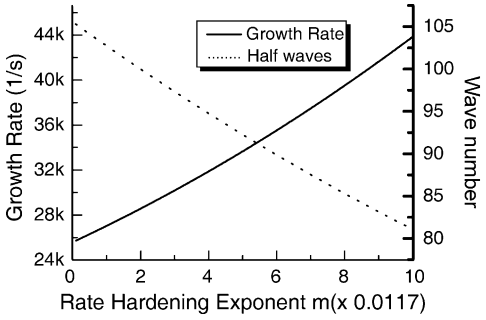

Fig. 9. The dependence of the maximum initial growth rate and the corresponding number of half-wavelengths along the plate length upon the strain rate hardening exponent, m.

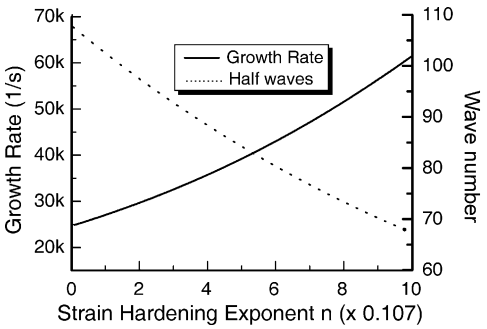

Fig. 10. The dependence of the maximum initial growth rate and corresponding number of half-wavelengths along the plate length upon the strain hardening exponent, n.

exponent from 0.107 to 1.07 increase wavenumbers by a factor of about 1.25 and 1.5, respectively. Thus the imposed axial strain-rate and the plate thickness influence strongly the wavelength of the buckled plate.

The approach followed here to study the stability of a prestressed thin plate is similar to that used by Bai [19] and others [20,21] for analyzing the stability of homogeneous simple shearing deformations of a thermoviscoplastic plate. In these studies a shear band is assumed to initiate as soon as an infinitesimal perturbation of a deformed state begins to grow. Batra and Chen [22] have shown numerically that the deformed state becomes unstable when the tangent modulus equals zero. In the present work, the tangent modulus equals zero for a perfectly plastic material and is a positive constant for a linearly strain hardening material. Thus the initial growth rate of perturbations for a rigid perfectly plastic plate is always positive, and is positive even for a strain-hardening rigid plastic material with realistic values of the hardening modulus. In the shear band problem [20,21,23] the wavelength corresponding to the maximum growth rate of initial perturbations determines the spacing between adjacent bands; here it determines the buckled shape of the plate. In [19–21], perturbations were not required to vanish wherever essential boundary conditions are given. In the present work, they vanish at points where essential boundary conditions are prescribed. Because of the thin plate theory used here, the possibility of instability induced by in-plane deformations has been eliminated. Hence, the onset of instability cannot correspond to the initiation of a shear band. We note that the present approach gives the correct buckling load for an elastic plate [24].

5. Conclusions

We have postulated that the wavelength of the infinitesimal perturbation superimposed upon an initially stressed plate corresponding to the maximum initial growth rate of the perturbation determines the buckled shape of the plate. The computed buckled shape is found to match well with that observed experimentally. For an orthotropic rectangular plate axially compressed on two opposite edges, the normal anisotropy strongly influences

the buckling mode. Both for isotropic and orthotropic plates, the wavenumber of the buckled plate increases with an increase in the applied axial strain-rate and a decrease in the plate thickness.

Acknowledgements

This work was partially supported by the ONR grant N00014-98-1-0300 to Virginia Polytechnic Institute and State University with Dr Y.D.S. Rajapakse as the cognizant Program Manager. Views expressed in the paper are those of authors and not of the funding agency.

References

[1] Jones N. Structural impact. Cambridge, MA: Cambridge University Press; 1989.
[2] Illyshin AA. The elastic plastic stability of plates. NACA TM 1188; 1947.
[3] Stowell EZ. A unified theory of plastic buckling of columns and plates. NACA TN 1156; 1948.
[4] Bijlaard PP. Theory and tests on the plastic stability of plates and shells. J Aeronaut Sci 1949;9:529–41.
[5] Handelman GH, Prager W. Plastic buckling of rectangular plates under edge thrusts. NACA TN 1530; 1948.
[6] Pride RA, Heimerl GJ. Plastic buckling of simply-supported compressed plates. NACA TN 1817; 1949.
[7] Pearson CE. Bifurcation criterion and plastic buckling of plates and columns. J Aeronaut Sci 1950;7: 417–26.
[8] Neale KW. Effect of imperfection on the plastic buckling of rectangular plates. J Appl Mech 1975;42: 115–20.
[9] Needleman A, Tvergaard V. An analysis of the imperfection sensitivity of square elastic plastic plates under axial compression. Int J Solids Struct 1976;12:185–201.
[10] Tvergaard V. Rate sensitivity in elastic–plastic panel buckling. In: Sawe DJ et al, editor. Aspects of the analysis of plate structures. Oxford: Clarendon Press; 1985. p. 293–308.
[11] Paley M, Aboudi J. Viscoplastic bifurcation buckling of plates. AIAA J 1991;29:627–32.
[12] Simitses GJ, Song Y. Thermo-elastoviscoplastic buckling behavior of plates. J Appl Mech 1994;61:169–75.
[13] Goodier J.N. Dynamic buckling of rectangular plates and sustained plastic compressive flow, in Engineering Plasticity, Cambridge University Press; 1968: 183–200, Proceedings of an international conference on plasticity held in Cambridge, England, March 1968.
[14] Lindberg HE, Florence AL. Dynamic pulse buckling—theory and experiments. Leiden: Martinus Nijhoff; 1987 p. 349–72.
[15] Batra RC, Geng TS. Enhancement of the dynamic buckling load for a plate by using piezoceramic actuators. Smart Mater Struct 2001;10:925–33.
[16] Batra RC, Geng TS. Comparison of active constrained layer damping by using extension and shear mode actuators. J Intell Mater Struct 2002;13(6):349–67.
[17] Hill R. The mathematical theory of plasticity. Oxford: Oxford University Press; 1950.
[18] Batra RC, Jaber NA. Failure mode transition speeds in an impact loaded prenotched plate with four thermoviscoplastic relations. Int J Fract 2001;110:47–71.
[19] Bai YL. Thermoplastic instability in simple shear. J Mech Phys Solids 1982;30:195–207.
[20] Chen L, Batra RC. Effect of material parameters on shear band spacing in work-hardening gradient-dependent thermoviscoplastic materials. Int J Plasticity 1999;15:551–74.
[21] Batra RC, Chen L. Instability analysis and shear band spacing in gradient-dependent thermoviscoplastic materials with finite speeds of thermal waves. Arch Mech 2001;53:167–92.

[22] Batra RC, Chen L. Effect of viscoplastic relations on the instability strain, shear band initiation strain, the strain corresponding to the minimum shear band spacing, and the band width in thermoviscoplastic materials. Int J Plasticity 2001;17:1465–89.
[23] Batra RC, Wei ZG. Shear band spacing in thermoviscoplastic materials. Int J Impact Eng (available online).
[24] Wei ZG, Batra RC. Buckling of precompressed elastic plates due to continuous laser heating. In: Librescu L, Marzocca P, editors. Proceedings of the 5th international congress on thermal stress and related topics, Blacksburg, June 2003, paper #MM-1-1.